Particle migration in a concentrated suspension flowing between rotating parallel plates: Investigation of diffusion flux coefficients

Dima Merhi

Laboratoire de Technologies des composites, Ecole Polytechnique Fédérale de Lausanne, CH1015-Switzerland

Elisabeth Lemaire^{a)} and Georges Bossis

Laboratoire de Physique de la Matière Condensée, CNRS-UMR6622, Parc Valrose, 06108 Nice cedex2 France

Fadl Moukalled

American University of Beirut, Faculty of Engineering & Architecture, Mechanical Engineering Department, P.O.Box 11-0236, Riad El Solh, Beirut 1107 2020 Lebanon

(Received 13 May 2005; final revision received 26 August 2005)

Synopsis

This paper reports an experimental and numerical study conducted to investigate the behavior of macroscopic monomodal concentrated suspensions (40%) undergoing a creeping torsional flow between two rotating plates. An experimental technique based on the detection of tracers by measurement of light absorption is developed and used to quantify the time evolution of the particles concentration profiles. Contrarily to results reported in the literature, an outward migration of the particles is observed. This shear-induced migration is confirmed by viscometric measurements where an increase in the apparent viscosity of the suspension has been observed for long periods of shear. Moreover, this increase is found to depend solely on the value of the applied strain, which is consistent with a shear-induced migration phenomenon. Experimental results are reproduced using a semi-quantitative model involving the balance of three diffusion fluxes induced, respectively, by the gradient of viscosity (J_n) , the gradient of the collision rate between particles (J_c) , and the flow curvature (J_r) . Steady and transient numerical profiles are obtained using a finite volume approach. The coefficients of the diffusion fluxes (K_n, K_c, K_r) are determined by optimizing the numerical profiles to fit the experimental data. The ratios of these coefficients (K_n/K_c) and K_r/K_c) are found to be independent of the flow geometry with their absolute values being tightly coupled to the direction of particles drift. In particular, the migration coefficients in the direction of the velocity gradient (in a cylindrical Couette flow) are found to be almost five times larger than those along the direction of vorticity (in a rotating parallel-plate flow). © 2005 The Society of Rheology. [DOI: 10.1122/1.2079247]

a) Author to whom correspondence should be addressed; electronic mail: elisabeth.lemaire@unice.fr

I. INTRODUCTION

Hydrodynamic interactions between noncolloidal particles of a concentrated suspension flowing at low Reynolds number are responsible for macroscopically observed effects, such as viscous resuspension [Leighton and Acrivos (1986)], particle segregation, and particle migration [Leighton and Acrivos (1987)]. This latter effect—often referred to as shear induced migration—was first observed by Karnis *et al.* (1966) who reported blunted velocity profiles for suspensions flowing through a tube. However, the particles volume fraction profiles were not quantitatively determined.

Later, Gadala-Maria and Acrivos (1991) reported that the apparent shear viscosity of a concentrated suspension of non-Brownian neutrally buoyant particles flowing in a Couette viscometer decreases with time during prolonged shearing at low shear rates. Leighton and Acrivos (1987) attributed this decrease to a shear-induced migration of particles across the gap from high shear stress regions to low shear stress regions. Several experimental observations using different techniques confirmed that particle migration often takes place in flowing suspensions. Using nuclear magnetic resonance imaging (NMRI), Abbott *et al.* (1991) found that particles migrate away from the inner cylinder toward the outer one where the shear rate is lower. They measured a migration rate proportional to the shear rate and to the 2.7 ± 0.3 power of the mean particle diameter of sieved particles. Chow *et al.* (1994) and Phillips *et al.* (1992) carried out experiments in Couette flow geometry with a large reservoir. Their NMRI profiles showed similar results concerning the radial migration. Furthermore, Chow *et al.* (1994) noticed that during shearing, particles moved to the reservoir where they experienced a lower shear rate.

Other experiments have been performed for pressure driven flows where the concentration profiles have been determined either by NMRI [Hampton *et al.* (1997); Sinton *et al.* (1991); Altobelli *et al.* (1991)] or by laser Doppler anemometry (Koh *et al.* (1994); Lyon and Leal (1998)]. All of these studies reported the demixion of the initially homogenous suspension and a blunted velocity profile associated with an increase of the particles concentration at the center of the conduit.

The interpretation of the shear-induced migration is still controversial. Two noteworthy theories have been proposed to explain the irreversible motion of particles under inhomogeneous shear rate. The first one, introduced by Jenkins and McTigue (1990), is based on the conservation of mass and momentum and the fluctuational energy for the particular phase. This approach inspired Nott and Brady (1994)—who linked the suspension pressure to the fluctuational motion of particles in order to introduce nonlocality in the description of suspension behavior and remove the difficulties in regions of zeroshear rate. In this model, they derived an energy balance equation and solved it simultaneously with the momentum and the mass conservation equations for both particle and suspension phases, also they incorporated normal stresses in the constitutive equations. Therefore, there is no diffusive motion of particles which are considered as a material phase, and migration occurs through the requirement that the macroscopic pressure is constantly perpendicular to the direction of mean motion. However, it is rather difficult to implement this model in a numerical solver due to the lack of an explicit convectiondiffusion equation for the volume fraction. Even with the improved boundary condition suggested by Morris and Brady (1998) to prevent the unrealistic increase of particle concentration on solid surfaces, numerical predictions did not agree well with experimental data [Fang and Phan-Thien (1999)]. In a similar attempt Mills and Snabre (1995) introduced nonlocality through the formation of a particle network and ascribed migration to long-range hydrodynamic interactions and spatial variation of the local stress tensor.

Inspired by Nott and Brady's approach (1994) as well, Morris and Boulay (1999) derived a rheological model for steady shear of noncolloidal suspensions including the normal stresses. They established an equation that may predict the conditions required for a particle's migration in curvilinear flows in terms of normal stresses ratios that are independent of the particle volume fraction. In this case, the entire dependence on particle volume fraction is captured by a "normal stress viscosity" and the nonlocality aspect is introduced via a supplementary isotropic stress that is a function of the shear rate gradient and the normal viscosity.

On the other hand, a class of phenomenological models have been developed to describe the shear-induced migration. Leighton and Acrivos (1987) attributed migration to irreversible interactions due to the particles surface roughness. Indeed, earlier experiments by Arp and Mason (1977) showed that even a slight surface roughness (10⁻⁴ radius) could lead to asymmetric trajectories of two colliding spheres. In their model, Leighton and Acrivos (1987) assumed the existence of two migration fluxes. The first one, called the collision flux, represents the drift of particles toward regions where the collision rate is lower and is given by

$$J_c = -K_c a^2 \Phi \nabla (\dot{\gamma} \Phi), \tag{1}$$

where a is the particle radius, $\dot{\gamma}$ is the shear rate, Φ is the concentration of the solid phase, $a\nabla(\dot{\gamma}\Phi)$ is the variation of the collision rate over a distance of the order of a, and K_c is the dimensionless diffusion coefficient of the collision flux.

The second flux is the viscosity flux, which can be present if there exists a particle concentration gradient and thus through a spatial variation of the viscosity. This particle flux is directed from the high to low viscosity regions. Assuming that the drift velocity is proportional to the change in viscosity over a distance O(a), the viscosity flux \mathbf{J}_{η} may be written as

$$J_{\eta} = -K_{\eta} a^2 \dot{\gamma} \frac{\Phi^2}{\eta} \nabla \eta, \qquad (2)$$

where K_{η} is the dimensionless diffusion coefficient of the viscosity flux, and η the effective viscosity of the suspension.

However, the above model failed to explain why Chow *et al.* (1994) observed an outward migration in cone plate geometry, in spite of a constant shear rate. Furthermore, Krishnan *et al.* (1996) and Chapman (1990) noted that in curved geometries one could not ignore the influence of the streamlines curvature on particles motion. Based on these observations, Krishnan *et al.* (1996) proposed a third flux called the curvature flux, J_r to account for this effect. Since particles interacting in a shear field with curved streamlines migrate toward regions of lower curvature, they expressed the outward curvature flux as

$$J_r = +K_r \dot{\gamma} a^2 \frac{\Phi^2}{r}.$$
(3)

The plus sign indicates that this flux is in the opposite direction of the previous ones. The balance of the above three fluxes leads to the steady spatial distribution of the particles. In this approach, the dimensionless diffusion coefficients K_c , K_η , and K_r are adjustable parameters that have to be evaluated by comparing theoretical predictions against measured experimental concentration profiles. They represent the relative rates of the migration mechanisms and the final steady-state concentration profiles are uniquely determined by their ratio. This approach has the advantage of yielding relatively simple expressions that are capable of describing the complex phenomena associated with the shear-induced

migration in concentrated suspensions. Although the diagonal normal stresses are not explicitly represented in this model, they are "indirectly present" through particles anisotropic distribution. In fact upon shearing, nonhydrodynamic forces are developed in the system due to surface roughness. This leads to flow asymmetric interactions and therefore to an anisotropic microstructure. A nonsymmetric stress field is then induced and propagates throughout the fluid producing an imbalance in the bulk normal stresses.

Thus, studying the migration phenomenon through particles interactions and displacements captures the essential features of the particles' behavior and focuses on the origin of shear-induced migration itself.

Up until now, no clear evidence for particles' migration in a rotating parallel-plate flow has been found and it is currently assumed that the outward curvature flux quite exactly balanced the inward collision flux. Such a conclusion implies equal diffusion coefficients $(K_r = K_c)$ without any convincing argumentation. This paper reports on an experimental and numerical study to investigate particles' migration in concentrated suspensions flowing in a parallel-plate viscometer. The method is accurate enough to determine even low concentration gradients. We show first experimental evidence on particle migration in parallel-plate geometry. From the steady concentration profiles, the relative magnitudes of the fluxes, or equivalently the associated diffusion coefficients, are determined. The curvature flux is shown to have a higher impact on particles' drift than the collision flux. In addition, shear-induced diffusion coefficients are proven to be spatially anisotropic and, therefore, to depend greatly upon the particles' drift direction in curved geometries. Results are validated by demonstrating that the coefficient ratios, K_r/K_c and K_η/K_c , determined in a parallel-plate geometry, represent the concentration profiles obtained by Phillips *et al.* (1992) in Couette flow geometry.

II. EXPERIMENTAL TECHNIQUES

A. Experimental procedure and setup

Several experimental techniques have been used to study the flow of concentrated suspensions including NMRI, laser Doppler anemometry, and ultrasound Doppler. However, most of these techniques require the implementation of cumbersome and expensive materials and have limited resolutions. To circumvent the problems encountered by previous experimental methods, a very simple and highly effective technique based on the detection of tracers by the measurement of light absorption is developed. The suspension is studied in a home-made shear cell depicted in Fig. 1. It consists of two 10 cm diameter glass disks, the upper disk is fixed and the lower one is driven at constant angular velocity by an engine. The distance between the disks is controlled by a micrometer with an accuracy of about 20 μ m and is set to one millimeter. In the conducted experiments, the angular velocity of the lower plate ranged between 18 rpm and 150 rpm, which corresponds to values of the Reynolds number between 8×10^{-4} and 7×10^{-3} , respectively. Thus, the flow is laminar and inertial forces are negligible as compared to viscous dissipation. The light source is a laser diode (Thorlabs Inc.) with a tuneable power up to 4 mW and a wavelength of 633 nm. The emitted light is detected by a photodiode (FDS100-Thorlabs Inc.) with a large active area of 13 mm². The laser beam and the photodetector are moved together in a radial direction from the outer edge of the disks toward the center, and the voltage signal of the photodiode is recorded. The initially loaded suspension is scanned in order to verify that the particle concentration has remained homogeneous during the filling process. Then, to shear the suspension, the lower disk is rotated at a constant spin rate. After a lapse of time, the rotation is switched off and the suspension is scanned again.

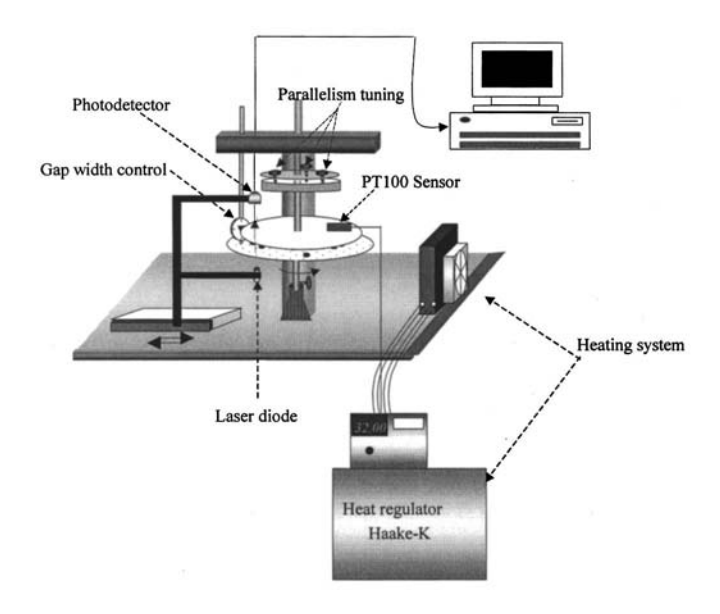


FIG. 1. Experimental setup for the observation of particles migration in rotating parallel-plate flow.

The light emitted by the laser diode is partially absorbed by the tracer particles and then detected by a photodiode that converts it into an electrical signal. The light source and the photodetector are mounted on a step-by-step engine of constant velocity v = 0.697 mm/s, which allows one to scan the cell along a specific radius. However, due to the presence of the axis of rotation, it is not possible to scan the central region of the cell $(R \le 20 \text{ mm})$. Therefore, the acquisition is made between $R_1 = 20 \text{ mm}$ and $R_2 = 45 \text{ mm}$.

In order to control the temperature, the device is placed in a thermostated box made of wood covered with 2 cm thick polyurethane sheets. The box is heated by a radiator connected to a thermostatic bath (Haake-K), which is controlled by a Pt-100 resistance thermometer located on the surface of the upper disk. To improve the homogeneity of the temperature in the box, a fan is placed behind the radiator.

B. Suspension

The suspension is made of 35% clear poly(methylmethacrylate) spheres (PMMA) and only 5% of tracer particles. The particles, obtained from ICI Acrylics, have a density of $1.18~\rm g/cm^3$ and, after sieving, their diameter is bounded between 200 and 250 μ m. Their surface roughness has been measured by electronic microscopy. One can see in Fig. 2, the existence of small excrescences that do not exceed 10^{-2} to 10^{-3} the radius but are sufficiently big to break the symmetry of the trajectory of two colliding particles. The tracers are obtained by infiltration of a PMMA adapted dye inside the clear particles. The dye (Macrolex blau) is dissolved in acetone, then water is added in order to minimize the corrosive effect of the solvent. The particles are then soaked in the mixture for 2 mins under constant mixing, and then rinsed thoroughly and dried in order to eliminate any residual content of the solvent. This process guarantees a persisting color inside the particles during long shear experiments and prevents the alteration of the particles surface aspect.

The suspending fluid must satisfy several constraints. First, it must be rather transparent because the followup of particles is done by light transmission. Moreover, to avoid

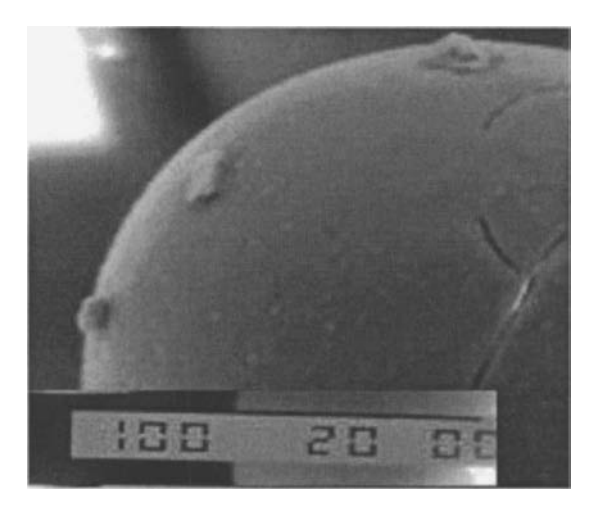


FIG. 2. Electronic microscopy picture of the surface of a PMMA particle.

sedimentation, centrifugal effects, and multiple scattering, the fluid should have the same density and refractive index as the particles. To fufill these conditions, a three-component liquid, similar to the one used by Krishnan *et al.* (1996), constituted of TritonX-100 (79.915%), ZnCl₂ (13.39%), and water (6.695%), is selected. The main disadvantage of this liquid is its low superficial tension which results in the formation of a multitude of air bubbles when it is mixed. As a consequence, it is necessary to eliminate these bubbles by ultrasonic degassing before each experiment.

C. Optimal operating temperature

The refraction index of the suspending liquid is very sensitive to temperature. Therefore, the matching depends on the accuracy with which the temperature of the suspension is determined and kept constant during the experiment. Moreover, it is crucial that the refraction index be matched at the particular laser wavelength used in the experiment, namely 633 nm. To exactly determine the temperature at which the transmitted light through the suspension maximizes, the transmission rate as a function of temperature $(T=29\ ^{\circ}\text{C}-38\ ^{\circ}\text{C})$, and the wavelength was measured using the experimental device depicted in Fig. 3(a).

As shown in Fig. 3(a), the studied suspension (1) is laid on a transparent slide and then introduced into a heating cell (2) connected to a temperature regulating system (8). The heating cell is put along with the sample on an Olympus BH-2 microscope (3). The transmitted light through the sample is collected via an objective and then analyzed by a monochrometer (4) adapted for the visible range $(0.5 \ \mu\text{m}-0.7 \ \mu\text{m})$. The value of the analyzed wavelength can be adjusted by modifying the position of the grating, which is controlled by an appropriate mechanical device (5). The analyzed light reaches a photomultiplicator (6), and is then converted into an electrical signal by an HP multimeter (7). For a fixed temperature, T, measurements of transmitted light were realized for wavelengths between 500 and 750 nm. After every measurement, the value of the transmission rate for λ =633 nm is selected. Figure 3(b) shows that the transmission at 633 nm maximizes at T=32 °C.

This temperature is high enough for the viscosity of the suspending liquid to be rather low (1.8 Pa s). However, keeping the suspension at this temperature for several hours

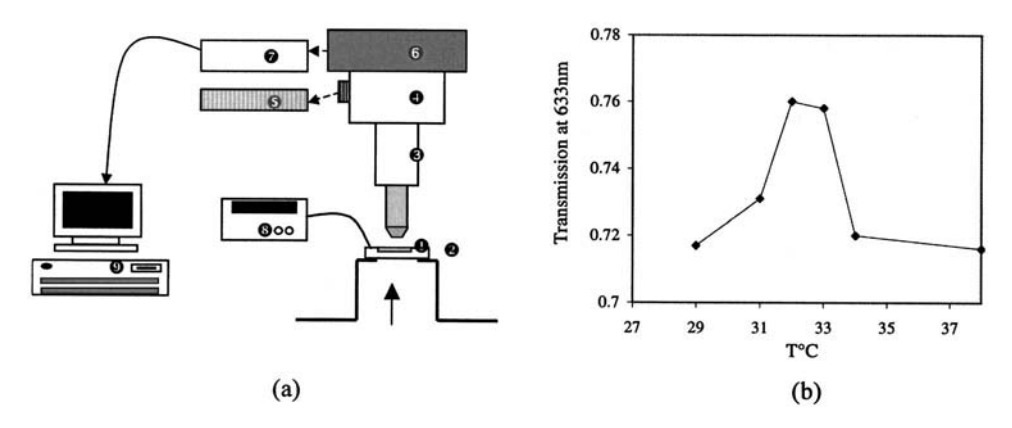


FIG. 3. (a) Experimental device for the measurements of transmission at λ =633 nm. (b) Transmission of light vs temperature for λ =633 nm through a 40% concentrated suspension.

implies the risk of evaporating the suspending fluid and mostly the water contained in it. This change in the fluid composition will modify the refraction index of the liquid. To avoid this problem, we built a system that can guarantee an airtight measure cell. This ensured reproducible measurements for short experiments (4–5 h). For longer experiments, we observed an alteration of the turbidity of the sheared suspension which means that this system is not effective for long shearing, it must be improved in order to have a complete sealing of the cell.

D. Turbidity experiments

In this section, it will be shown that neglecting scattering by the clear particles is justified considering the influence of the tracers on the transmission of light through the suspension.

The transmitted intensity by a suspension at time t=0, I_s^0 , is given by

$$I_s^0 = I_0 e^{-kx\Phi_m},\tag{4}$$

where I_0 is the intensity transmitted by the suspending fluid, Φ_m is the mean volume fraction of the particles, x is the suspension width, and k is a coefficient depending on the particles size and absorption. In order to avoid errors due to the attenuation of the beam by reflection on the plates or some parallelism defaults, the transmitted intensity at an instant t, I_s^t , is normalized by the first acquisition I_s^0 . The transmission rate is defined as $T = I_s^t/I_s^0$ and the value of the local concentration is calculated as a function of T, Φ_m , and x:

$$T = \frac{I_s^t}{I_o^t} = e^{kx(\Phi_m - \Phi)} \Rightarrow \Phi(r, t) = \Phi_m - \frac{1}{kx} \ln(T).$$
 (5)

Figure 4 compares the variation of transmission, as a function of the concentration of dyed particles, in two suspensions: The first one (Suspension I) contains 20% of clear particles and dyed particles whose concentration varies between 1 and 10%, while the second one (Suspension II) contains only dyed particles with the same volume fraction as in Suspension I.

We note that Suspension (I) presents a higher absorption than Suspension (II). However, this attenuation does not exceed 5% of the total absorption, which implies that the absorption of light by the tracers dominates widely the scattering by the white particles.

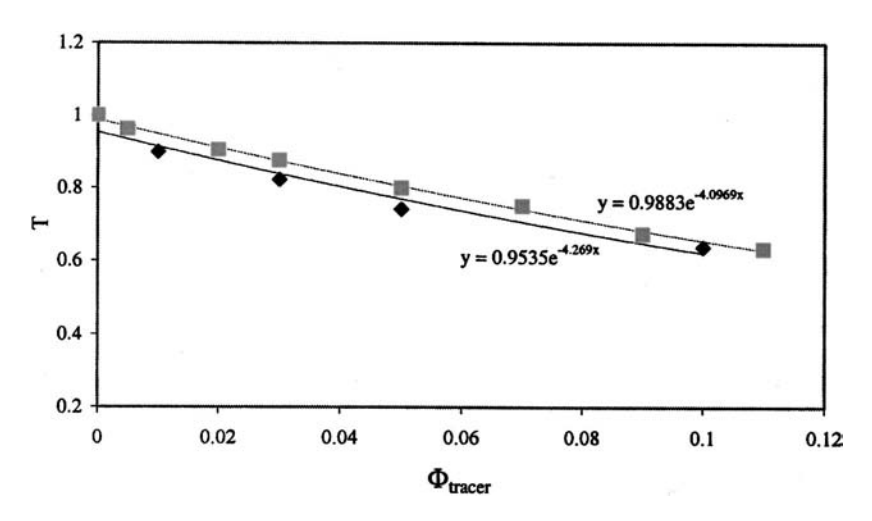


FIG. 4. Turbidity measurements versus the concentration of tracers particles for a suspension containing only the tracer particles (II) and a suspension containing the tracers plus 20% of clear particles (I).

III. EXPERIMENTAL RESULTS

A. Transient profiles of particles volume fraction: Light transmission measurements

The transmission measurements are made at t=0, 30, 60, 120, and 210 min for $\dot{\gamma}$ =40 s⁻¹ and Φ_m =40%. Figure 5 presents the initial and steady-state concentration profile reached after 210 min corresponding to a strain of value 5×10^5 and an inhomogeneous particle concentration profile. A significant migration of the particles is observed from the center to the periphery of the disks where the shear rate is higher and streamlines have lower curvature. The increase in volume fraction at the edge is almost 10% of its initial value. The complete variation ($\Delta\Phi_{\rm max} - \Delta\Phi_{\rm min}$) of particle concentration across the measured area is of 18%. The experimental profile shows local variation of the volume fraction values. These fluctuations have various origins as the local variation of the

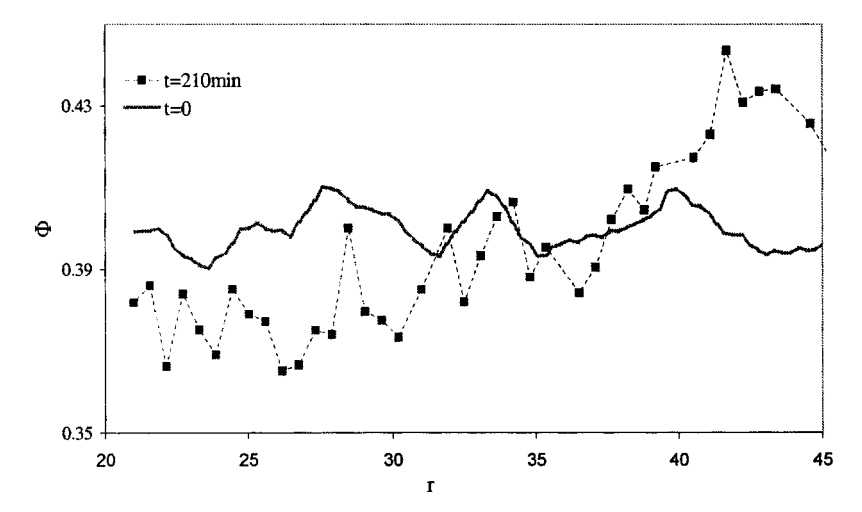


FIG. 5. Steady-state profile reached after 210 min for Φ =40% and $\dot{\gamma}$ =40 s⁻¹.

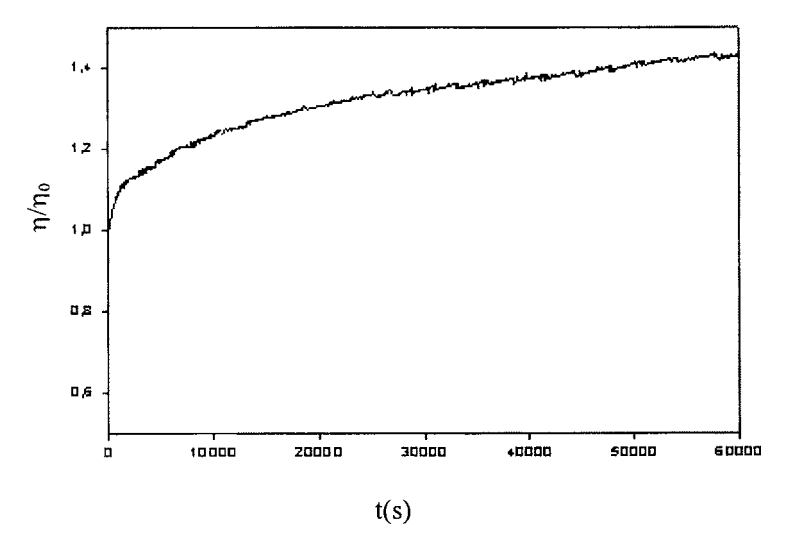


FIG. 6. Normalized viscosity of the suspension vs time for $\Phi=40\%$ and $\dot{\gamma}=40~{\rm s}^{-1}$.

refractive index of the suspension or fluctuations resulting of the finite particle size effect fitting across the gap and short time oscillations of the laser beam. In any case, these variations in local particle concentrations are bounded between 1.7 and 5%, which is sufficiently lower than the 18% observed across the disk. In Couette flow, the experimental profiles obtained by Phillips *et al.* (1992) show almost a 40% absolute variation of the particles volume fraction. Thus, the intensity of the migration in this geometry is almost twice that in parallel plate which may explain why, in NMR measurements, authors succeeded in noticing shear-induced migration for the former and not for the latter geometry.

B. Torque measurements

Viscometric measurements are carried out in the same geometry using a Carrimed CSL100 rheometer. The suspension used for torque measurements consists of particles of smaller diameter $10\pm1~\mu m$ (Bangslabs) concentrated up to 40% in the same suspending fluid as in the light transmission experiments. The particles used in this set of experiments are smaller than the ones used in the light transmission experiments as the rheometrical device is smaller in this case. Besides, these small particles are highly monodisperse which will prevent any false interpretation of the results due to particles size segregation. The suspension is introduced into the gap (fixed at $500~\mu m$) between the two parallel disks. It is very sensitive to moisture, evaporation, and temperature fluctuations. Its behavior may change during the experiment if the composition of the suspending liquid changes. Therefore, we had to isolate the setup completely, and carefully control the temperature to a precision of $0.1~^{\circ}C$.

The torque applied on the upper disk is given by

$$C = \int_{0}^{R} 2\pi r^{2} \tau(r) dr = 2\pi \frac{\Omega}{h} \int_{0}^{R} \eta(\Phi(r)) r^{3} dr.$$
 (6)

Figure 6 illustrates the general trends of the time dependent normalized torque during the flow and the effect of shear rate on the viscosity curve.

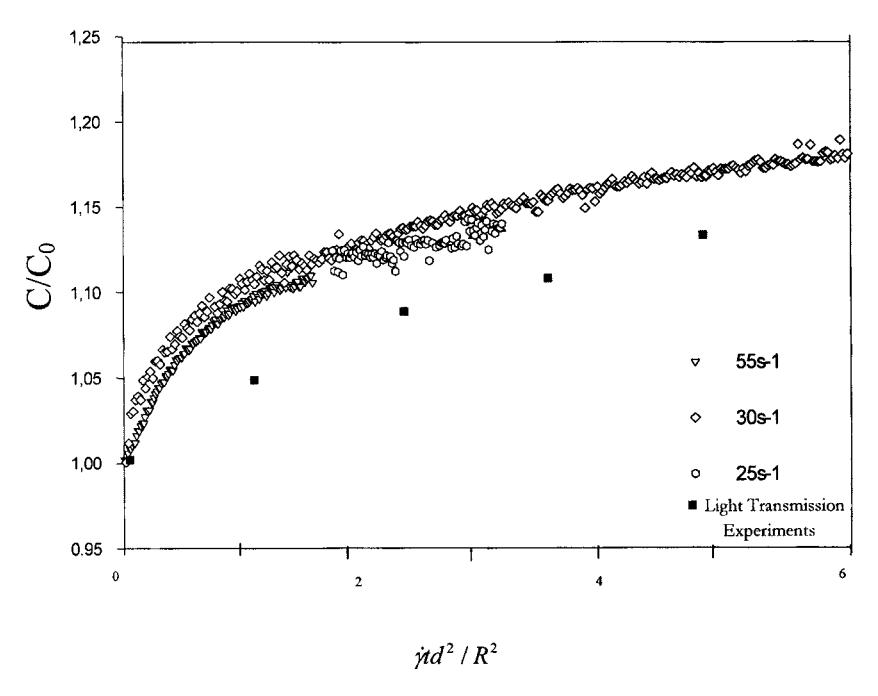


FIG. 7. Normalized torque values vs normalized strain values. Comparison between rheological tests and light transmission experiments.

After 16 h of shearing at 40 s⁻¹, the torque has increased by about 43% of the initial value indicating an increase in the volume fraction of the particles at the periphery and thus an outward shear-induced migration. To confirm that this increase is related to a migration phenomenon, several viscometric measurements have been made with different shear rates, and the measured normalized variation of the applied torque as a function of the normalized strain is plotted in Fig. 7. In particular, it is seen that the increase in the torque is identical for all shear rate values ($\dot{\gamma}=25~\text{s}^{-1}$, 30 s⁻¹, and 55 s⁻¹) and depends only on the applied strain. This fact is reflected by the unique curve obtained. These results are directly compared in Fig. 7 with the torque calculated from the values of $\Phi(r)$ obtained through light transmission experiments via the viscosity model. The curves show similar behavior in both experiments, however, a shift toward low torque values is observed for the calculated torque in light transmission experiments. An explanation would be the rheological law used to calculate the viscosity values. In fact, this law might not accurately describe the behavior of the studied suspension. A more precise estimation of the maximum packing volume fraction and the exponent would most probably lead to better estimation of the torque. Nevertheless, these results confirm that shear inducedmigration observed in light absorption technique corresponds to an increase of the torque with the applied strain.

These results are contradictory to experimental observations reported in the literature in this geometry. Indeed, the previous studies concerning the migration of particles in monodisperse suspensions in parallel-plate geometry did not reveal any significant change in the particle distribution in parallel-plate flow. However, it should be mentioned that Chow *et al.* (1994) have made the only direct measurement of the concentration profiles in this geometry using NMRI technique, which is not accurate enough to reveal such a low concentration gradient as air bubbles give the same signal as solid particles.

Furthermore, the migration is very slow and its long characteristic time explains why Chapman (1990) did not observe any migration during his rheological measurements.

IV. NUMERICAL MODELING

This section presents the numerical calculation procedure used to compute the concentration profiles based on the model described in the Introduction. This model is easily adapted to predict particles behavior in various systems and flow patterns, thereby serving as a handy tool to design and analyze experiments.

After the presentation of the constitutive equations, a brief description of the numerical method and algorithm used in the simulations is given. The benchmarking between the numerical results and experimental profiles is then discussed in Sec. IV.

A. Basic equations

1. Conservation equations

Though the particle migration leads to a nonuniform distribution of particles across the flow field, the density of the suspension remains constant since the particles are neutrally buoyant. Considering the suspending fluid as Newtonian and incompressible, the total stress in the suspension is given by

$$\tau = \eta(\Phi)\dot{\gamma}.\tag{7}$$

The mass and momentum conservation equations can be written as

$$\nabla \cdot \mathbf{v} = 0, \tag{8}$$

$$\frac{\partial}{\partial t}(\rho \mathbf{v}) + \nabla \cdot (\rho \mathbf{v} \mathbf{v}) = \nabla \cdot (\eta \nabla \mathbf{v}) - (\nabla \mathbf{P}) + \mathbf{S}$$
(9)

where \mathbf{v} is the velocity vector, $\boldsymbol{\eta}$ is the viscosity of the suspension, P is the pressure, and \mathbf{S} is the source term, which includes all the volume forces, applied to the suspension. The convection term in this equation is not linked to the experimental work achieved in this study as we are concerned with laminar flow fields. However, the equation is kept in this form in order to be implemented for more general flow fields in the numerical solver.

2. Diffusion equation

Based on the expressions of the diffusive fluxes described in the Introduction, the time evolution of the solid particles concentration profile is given by

$$\frac{\partial \Phi}{\partial t} = -\frac{\partial}{\partial r} \left\{ K_c \Phi a^2 \nabla (\Phi \dot{\gamma}) + K_{\eta} a^2 \dot{\gamma} \frac{\Phi^2}{\eta} \nabla \eta - K_r \dot{\gamma} a^2 \frac{\Phi^2}{r} \right\}. \tag{10}$$

The momentum and concentration equations are coupled through a concentration dependent relative viscosity. Various models for the viscosity of concentrated suspensions are available [Kreiger and Dougherty (1959); Probstein *et al.* (1994); Cohen *et al.* (1997)], the particular choice of any of these models is not expected to affect the solution qualitatively. Using the empirical expression for the viscosity suggested by Krieger and Dougherty (1959), the relative viscosity of the suspension is given by

$$\eta_s = \left(1 - \frac{\Phi}{\Phi_m}\right)^{-1.82},\tag{11}$$

where Φ_m is the maximum packing concentration for a monodisperse suspension which is assumed to be equal to 0.68.

At steady state, $\frac{\partial \Phi}{\partial t} = 0$ hence,

$$\frac{1}{\dot{\gamma}}\nabla\dot{\gamma} + \frac{1}{\Phi}\nabla\Phi + \frac{K_{\eta}}{K_{c}}\frac{1}{\eta}\nabla\eta - \frac{K_{r}}{K_{c}}\frac{1}{r} = 0.$$
 (12)

Integrating Eq. (12), one obtains the following relation between the local variables $(r, \eta, \Phi, \dot{\gamma})$ and their boundary values $(R_w, \eta_w, \phi_w, and \dot{\gamma}_w)$:

$$\frac{\dot{\gamma}\Phi}{\dot{\gamma}_w\Phi_w} = \left(\frac{\eta_w}{\eta}\right)^{k_\eta} \left(\frac{r}{R_w}\right)^{k_r},\tag{13}$$

where $k_{\eta} = \frac{K_{\eta}}{K_c}$ and $k_r = \frac{K_r}{K_c}$. To calculate the transient profiles, Eq. (10) is solved using the finite volume method outlined next.

B. Numerical method

Numerical profiles are generated using a finite volume technique devised by Patankar (1980). Finite volume methods have gained a wide popularity due to their conservative properties and modest storage and computational effort requirements making it possible to simulate complex problems on desktop workstations. The starting point of this method is to write all governing equations in the form of a general transport equation for the field variable Φ as

$$\frac{\partial(\Pi\Phi)}{\partial t} + \nabla \cdot (\Pi \mathbf{v}\Phi) = \nabla \cdot (\Gamma \nabla \Phi) + S_{\Phi}, \tag{14}$$

where $\Gamma \nabla \Phi$ is the diffusion flux of the scalar variable Φ , S_{Φ} is the source term, and $\Pi \mathbf{v} \Phi$ is the convection flux. The expressions for Π , Γ , and S_{Φ} for a particular meaning of Φ can be deduced from the parent equation.

In this procedure, the solution domain is subdivided into a number of control volumes with a grid point located at their centers. Integrating Eq. (14) over a cell of volume *V* bounded by Surface A and applying the divergence theorem, the following conservation equation in integral form is obtained:

$$\int_{V} \frac{\partial}{\partial t} (\Pi \Phi) dV + \oint_{A} \Pi(v_{i} \Phi) \cdot n_{i} dS = \oint_{A} \Gamma(\nabla \Phi) \cdot \mathbf{n} dS + \int_{V} S_{\Phi} dV, \tag{15}$$

where \mathbf{n} is the outward unit normal vector.

With suitable profile interpolation in each coordinate direction for the variables whose values are unknown on the control volume faces, Eq. (15) is transformed into the following algebraic equation:

$$a_{p}^{t}\Phi_{p}^{t} = \sum_{nh} a_{nh}^{t}\Phi_{nh}^{t} + a_{p}^{0}\Phi_{p}^{t-\Delta t} + b^{t},$$
(16)

where the subscript P represents the current node, the subscript nb is the neighboring nodes to the P grid point, t is the current time, Δt is the time step, and the coefficients a_P^t , a_{nb}^t , and a_P^0 are found from grid geometry and the current kinematics. A similar equation results at each P grid point and the set of these equations forms a system of nonlinear

algebraic equations that is solved iteratively using a line-by-line Thomas algorithm [Patankar (1980)].

V. DETERMINATION OF THE DIFFUSION COEFFICIENTS

In this section, the theoretical predictions obtained by solving the phenomenological constitutive equation are compared against the experimental concentration profiles. At steady state, the tuning parameters are the coefficient ratios $k_{\eta}=K_{\eta}/K_c$ and $k_r=K_r/K_c$. In order to fit their experimental profiles, Phillips *et al.* (1992) did not take into account the existence of the curvature flux, hence the only influencing parameter considered was K_{η}/K_c , which was found to be of 0.66. On the other hand, Krishnan *et al.* (1996) did not observe significant spatial variation of particles volume fraction and hence suggested that the inward collision flux balances quite exactly the outward curvature flux which implies that $K_r \approx K_c$. Tetlow *et al.* (1998) discussed the dependence of the magnitude of K_{η}/K_c on the local particle volume fraction and found that for concentrated suspensions flowing in a wide Couette device, this ratio can be modeled as a linear function of the local particle concentration. However, they did not take into consideration the influence of streamlines curvature on particle drift in adjusting their parameter and, therefore, none of the reported values can model our experimental results.

A. Parallel-plate flow

In a parallel-plate device, the shear rate varies from zero at the center of the flow (r = 0) to its maximum value at the edge $(r = R_0)$, $\dot{\gamma}_0$:

$$\dot{\gamma} = \frac{r\Omega}{H},\tag{17}$$

where Ω is the angular velocity of the rotating plate (the upper one being fixed), and H is the gap width between the two plates.

The boundary condition on Φ is given by the conservation of the mean volume fraction of particles through the gap: $\bar{\Phi} = \frac{2}{R_0^2} \int_0^{R_0} r \Phi(r) dr$, and a no flux condition at the edge (**n.J**=0). All length scales are normalized by R_0 , velocities by $R_0\dot{\gamma}$ and time by $(R_0/a)^2/\dot{\gamma}_0 K_c$.

1. Steady-state profile

The values of k_r and k_η are obtained by fitting the experimental steady concentration profile with the numerical solution of Eq. (10). Figure 8 shows that the best numerical fit is obtained for $k_r = K_r / K_c = 1.95$ and $k_\eta = K_\eta / K_c = 2.1$.

2. Transient profiles: Determination of K_c

The transient profiles allow determining the value of K_c , the collision flux coefficient, and therefore to estimate the values of the three diffusion coefficients since their ratios are already known from the steady profiles. The simulations are performed using a dimensionless time step $\Delta \hat{t} = 3.2 \times 10^{-5}/K_c$. For a given transient experimental profile, a search is conducted to find the best numerical fit. Then identifying the numerical and experimental times, the value of K_c is evaluated and eventually those of K_r and K_{η} .

At a strain of $1.4 \times 10^5 (t_{\rm exp} = 60 \text{ min})$, the numerical fit is given for a time $t = 200/K_c$ (see Fig. 9). Comparing numerical and experimental times, one deduces the value of the collision diffusion coefficient: $t \approx t_{\rm exp} \Rightarrow K_c \approx 0.05$. Therefore, the migration coefficients in this geometry are found to be 0.105 for K_{η} and 0.0975 for K_{r} .

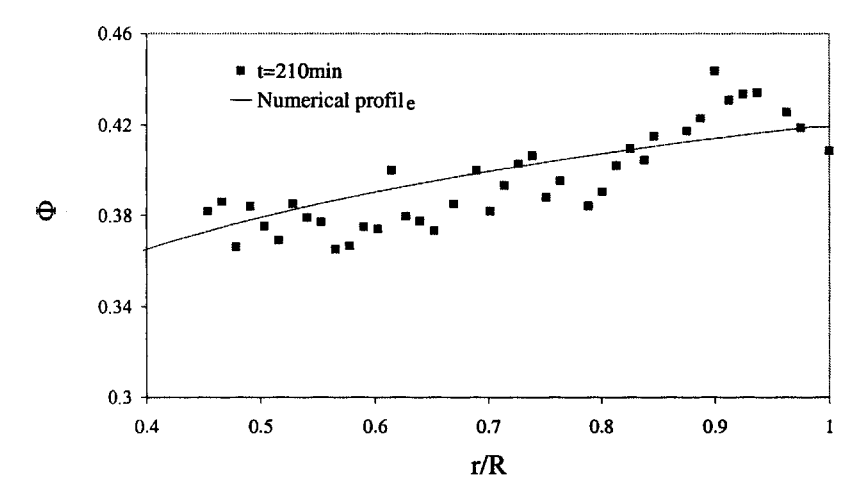


FIG. 8. Comparison between the steady experimental profile obtained in parallel-plate geometry and the best numerical fit for Φ =40%, K_r/K_c =1.95, and K_n/K_c =2.1.

The outward observed migration as well as the coefficients values indicate that the streamlines' curvature has a higher impact on the particle migration than on the shear rate gradient.

The relative magnitude of the migration coefficients, k_r and k_{rr} is expected to be the same for any rotational geometry. In particular, the results obtained in rotating parallel-plate flow should fit the steady profiles observed in Couette flow. To confirm it, numerical predictions in Couette flow using current parameters are compared next against experimental measurements reported by Phillips *et al.* (1992).

B. Couette flow

A Couette flow between two concentric cylinders ($\kappa = R_i/R_0$) separated by a large gap is considered. The inner cylinder rotates with an angular velocity Ω , while the outer

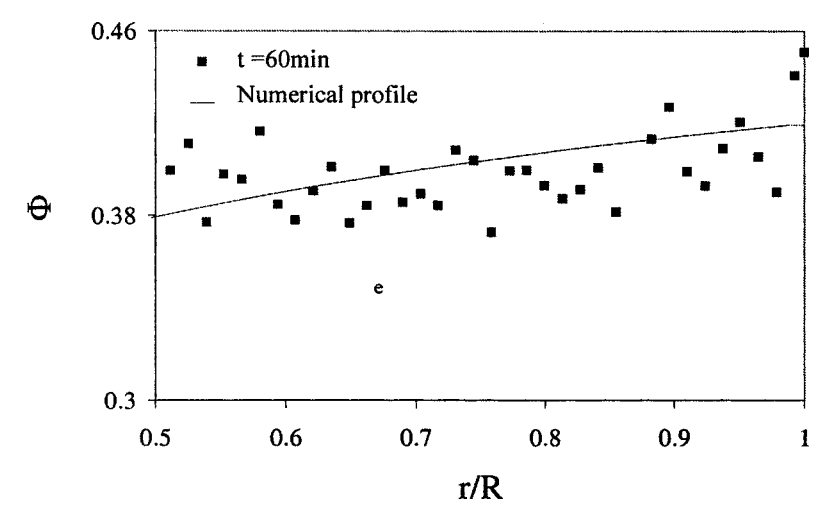


FIG. 9. Comparison between the transient experimental profile at $\gamma = 1.4 \times 10^5$ and the best numerical fit with $K_c = 0.05$, $K_{\eta} = 0.105$, and $K_r = 0.0975$.

cylinder is fixed. It is assumed that the cylinders are long enough for the flow to be unidirectional and that the variation of the particles concentration is only radial. The radial component of the momentum equation in cylindrical coordinates can be written as

$$\frac{1}{r^2} \frac{\partial}{\partial r} (r^2 \tau_{r\theta}) = 0 \Rightarrow \tau_{r\theta} = \frac{C}{r^2},\tag{18}$$

where C is an integration constant which depends on the geometry. The local shear rate is given by

$$\dot{\gamma} = C/r^2 \eta. \tag{19}$$

C is evaluated by writing $\dot{\gamma}$ in terms of the velocity v_{θ} to obtain:

$$\dot{\gamma} = r \frac{d}{dr} \left(\frac{v_{\theta}}{r} \right) = \frac{C}{mr^2}.$$
 (20)

Integrating Eq. (20) from the inner to the outer wall and with no-slip conditions at the solid boundaries yields:

$$C = \frac{-\Omega}{\int_{\kappa R_0}^{R_0} (1/r^3 \eta) dr},\tag{21}$$

with the shear rate computed using Eqs. (20) and (21), Eq. (10) is solved using the finite volume numerical procedure described earlier to predict the time evolution of the concentration profiles.

In the following, using the previously established coefficients ratios, theoretical predictions are compared against the experimental profiles obtained by Phillips *et al.* (1992) for a suspension flowing in a large gap Couette device with an average volume fraction of 55% and average particle diameter of 675 μ m.

1. Steady-state profile

Substituting $\dot{\gamma}$ in Eq. (13) by its expression given by Eq. (20), we obtain an equation with two tuning parameters k_{η} and k_{r}

$$\frac{\Phi}{\Phi_w} = \left(\frac{\eta_w}{\eta}\right)^{k_{\eta}-1} \left(\frac{r}{R_w}\right)^{k_r+2}.$$
(22)

Using Krieger's and Dougherty empirical expression for the relative suspension viscosity, the following expression for the steady concentration profile is derived:

$$\frac{\Phi}{\Phi_w} = \left(\frac{1 - \Phi_w/0.68}{1 - \Phi/0.68}\right)^{1.82(1 - k_\eta)} \left(\frac{r}{R_w}\right)^{k_r + 2}.$$
 (23)

Equation (23) is used in conjunction with the following particles average volume faction condition:

$$\bar{\Phi} = \frac{2}{R_{\text{max}}^2 - R_{\text{min}}^2} \int_{R_{\text{min}}}^{R_{\text{max}}} r \Phi(r) dr \tag{24}$$

to iteratively update the particle concentration at the walls (Φ_w) during the numerical solution of Eq. (10).

Phillips et al. (1992) conducted NMRI measurements on the same geometry and performed simulations of the steady-state and transient profiles. The experimental results

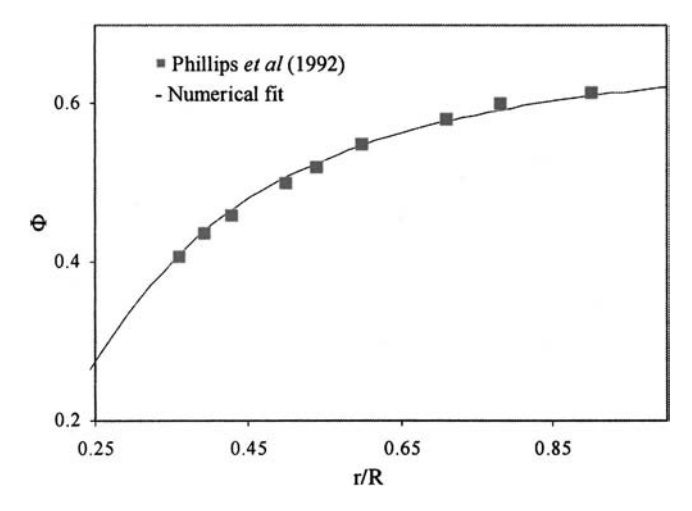


FIG. 10. Benchmarking between Phillips *et al.* (1992) experimental steady profile in Couette flow (\blacklozenge) and the numerical steady profile (—) obtained with $K_r/K_c=1.95$, $K_n/K_c=2.1$ and $\Phi=55\%$.

definitely show the presence of shear-induced migration through highly nonuniform particle concentration profiles at steady state, with maximum concentration near the outer wall. The steady state was reached after 800 revolutions of the inner cylinder.

Figure 10 presents a comparison between Phillips *et al.* (1992) experimental profile and current numerical predictions using the diffusion coefficient ratios $(k_r = K_r/K_c = 1.95)$ and $k_\eta = K_\eta/K_c = 2.1$) determined in parallel-plate geometry. The very good agreement is a validation of the values obtained for both ratio values, k_r and k_η and confirm as well that experimental profiles obtained with transmission light technique are correlated to profile obtained with NMR on a different rotational geometry by the same diffusion coefficient ratios.

2. Transient profiles: Determination of K_c

Figure 11 presents the time evolution of the concentration profiles obtained with an integration dimensionless time step of $\Delta \hat{t} = 1.6 \times 10^{-5}$ normalized by the characteristic time $\tau = (R_0/a)^2/K_c\Omega$ with $a/R_0 = 2 \times 10^{-2}$ and $\Omega = 17$ rpm. Numerical profiles show particle migration from the inner cylinder toward the outer cylinder and very weak evolution of the concentration profiles after 640 revolutions. The steady state is independent of Ω , the rotational velocity of the inner cylinder, only the number of revolutions $n = \Omega t/2\pi$ is significant.

Comparing current predictions to Phillips *et al.* (1992) transient profiles, we obtain the best fit of the experimental data as $K_c \approx 0.25$ —which leads to a viscosity coefficient K_η of 0.525 and a curvature coefficient K_r of 0.487. For these values, it is possible to numerically reproduce all transient experimental profiles for n=50, 100, 200, and 800 revolutions.

3. Discussion

The opposite directions of the collision and the curvature fluxes explains why, in a torsional flow, the magnitude of the migration is much smaller than in a Couette flow geometry. Furthermore, in the former geometry, the migration is much slower. Indeed, despite the fact that the coefficient ratios used to fit the steady-state profiles in Couette

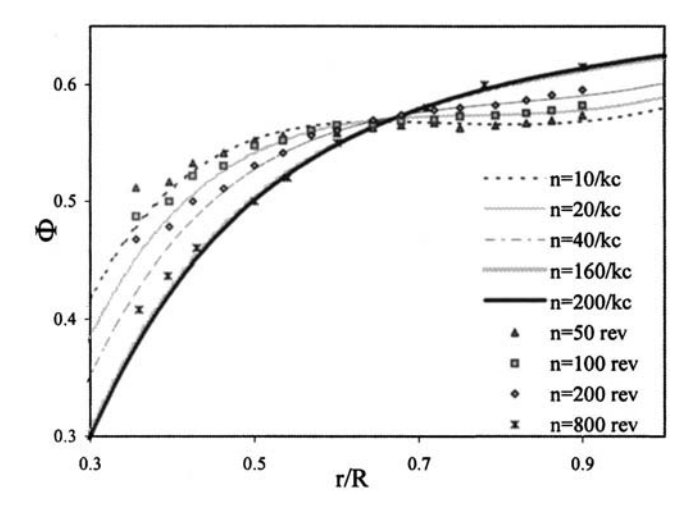


FIG. 11. Numerical fit of Phillips et al. (1992) experimental transient profiles in Couette flow device.

and parallel-plate flow are the same, the absolute value of the three coefficients are clearly different. The diffusion coefficients are about five times higher in Couette flow than in parallel-plate geometry. This is not a surprising result since the diffusion coefficients values are expected to depend on the particles' interaction rate and particles' deviation after each collision—which is very different whether the particles drift is parallel or perpendicular to the plane of shear.

In fact, particles' migration occurs in the plane (r, θ) , along the velocity gradient direction, in Couette flow where the particles' drift is higher than that in the direction of vorticity, which is the particles' drift direction in parallel-plate flow. This observation may be connected to previous studies concerned with self-diffusion process of colloidal and non-Brownian spheres. These include the experimental work for shear-induced selfdiffusion of non-Brownian particles [Leighton and Acrivos (1987); Breedveld et al. (1998)], computations via Stokesian dynamics simulations [Bossis and Brady (1987); Pesche (1998); Phung (1993)] and the theoretical work preformed by Brady and Morris (1997) and da Cunha and Hinch (1996). The latter performed pair trajectory calculations to evaluate both the shear-enhanced and down gradient diffusivities in a dilute sheared suspension of spheres with small-scale surface roughness. They, predicted that the diffusion in the direction of velocity gradient (D_{\parallel}) is almost one order of magnitude greater than that in the direction of vorticity (D_{\perp}) . Brady and Morris (1997) analyzed the pair distribution function under the combined influence of weak Brownian motion and an interparticle force of hard-spheres type. The magnitude of the predicted diffusivities in the vorticity direction were very similar in both approaches, and both studies found the diffusivity in the velocity gradient direction to be much larger than in the vorticity direction. On the other hand, experimental measurements of particles self-diffusivity in concentrated suspensions [Breedveld et al. (1998)] have displayed a ratio of about 1.7 between the two coefficients. It is noteworthy that the coefficients of self-diffusion are quite different from the shear-induced collective diffusivity especially at high concentrations where the particles interactions become important. This may explain the scatter with the value obtained for the ratio of both coefficients in this study comparing to the ones estimated through theory or experimental work concerned with self-diffusivity. However,

even if self-diffusion and collective diffusion represent distinct physical processes, we believe that they have the same origin which is particles' drift due to surface roughness or equivalently short-range repulsive force.

VI. CONCLUSION

We present, in this study, first experimental evidence of the outward migration of particles in concentrated suspensions submitted to a flow between two parallel plates. The migration observed in this study implies that the outward curvature flux has a greater amplitude than the inward collision flux.

The experimental method based on light absorption is highly sensitive on tracers' volume fraction and allow the observation of a concentration gradient around 18% after 210 min of continuous shearing. This result is confirmed with the torque measurements on similar suspensions using a rheometric standard device with an accurate control of the temperature. The behavior of the macroscopic suspension was only strain dependent which confirmed a migration phenomenon.

Due to the low values of the diffusion coefficients in this geometry and to the antagonism in the flux directions, the migration characteristic time is much longer than in a Couette flow, and the steady particles concentration gradient is significantly lower. This fact may explain why previously reported experiments in the literature did not reveal any migration in this geometry.

Using the phenomenological model, we determined the values of the three diffusion coefficients through numerical simulations in both the parallel-plate flow ($K_c \approx 0.05$, $K_{\eta} \approx 0.105$, and $K_{r} \approx 0.0975$) and Couette flow ($K_c \approx 0.25$, $K_{\eta} \approx 0.525$, and $K_{r} \approx 0.487$). Furthermore, it was shown that their ratios ($K_{\eta}/K_{c}=2.1$ and $K_{r}/K_{c}=1.95$) fitted also the steady concentration profiles in both geometries. This result shows that the particles migration is spatially anisotropic, its magnitude being highly related to the particles drift direction. This model is quite easy to implement in a numerical solver and describes quite well the complex behavior of suspensions through particles interactions, even if it lacks possibilities when the general flow fields are considered.

These are promising results for monodisperse suspensions. Extensive experiments should be achieved using different volume fractions and particle diameters in order to establish whether this techniques is efficient for lower or higher volume fraction, and to study the dependence of diffusion fluxes with the particles size. Moreover, it would be interesting to have experimental profiles of other rotational geometries, such as cone plate, in order to verify that the migration coefficient ratios established in this study are independent of the studied rotational geometry. At present, experiments are conducted using bidisperse suspensions, the results will be discussed in a future publication.

References

Abbott, J. R., N. Tetlow, A. L. Graham, S. A. Altobelli, E. Fukushima, L. A. Mondy, and T. S. Stephens, "Experimental observations of particle migration in concentrated suspensions: Couette flow," J. Rheol. 35, 773–795 (1991).

Altobelli, S. A., R. C. Givler, and E. Fukushima, "Velocity and concentration measurements of suspensions by nuclear magnetic resonance imaging," J. Rheol. **35**, 721–734 (1991).

Arp, P. A. and S. G. Mason, "The kinetics of flowing dispersions. IX. Doublets of rigid spheres," J. Colloid Interface Sci. 61, 44-61 (1977).

Bossis, G., and J. F. Brady, "Self-diffusion of Brownian particles in concentrated suspensions under shear," J.

- Chem. Phys. 87, 5437-5448 (1987).
- Brady, J. F., and J. F. Morris, "Microstructure of strongly sheared suspensions and its impact on rheology and diffusion," J. Fluid Mech. 348, 103–139 (1997).
- Breedveld, V., A. T. van den Ende, and A. Acrivos, "The measurement of shear-induced particle and fluid tracer diffusivities in concentrated suspensions by a novel method," J. Fluid Mech. 375, 297–318 (1998).
- Chapman, B. K, "Shear-induced migration phenomena in concentrated suspensions," Ph.D. thesis, University of Notre Dame (1990).
- Chow, A. W., S. W. Sinton, J. H. Iwamiya, and T. S. Stephens, "Shear-induced migration in Couette and parallel-plate viscometers: NMR imaging and stress measurements," Phys. Fluids 6, 2561–2576 (1994).
- Cohen, E. G. D., R. Verberg, and I. M. Schepper, "Newtonian viscosity and viscoelastic behavior of concentrated neutral hard-sphere colloidal suspensions," Int. J. Multiphase Flow 23, 797–807 (1997).
- Da Cunha, F. R., and E. J. Hinch, "Shear-induced dispersion in a dilute suspension of rough spheres," J. Fluid Mech. 309, 211–223 (1996).
- Fang, Z., and N. Phan-Thien, "A particle suspension model: An unstructured finite-volume implementation," J. Non-Newtonian Fluid Mech. 80, 135–153 (1999).
- Gadala-Maria, F., and A. Acrivos, "Shear-induced structure in a concentrated suspension of solid spheres," J. Rheol. 24, 799–814 (1980).
- Hampton, R. E., A. A. Mammoli, A. L. Graham, N. Tetlow, and S. A. Altobelli, "Migration of particles undergoing pressure driven flow in a circular conduit," J. Rheol. 41, 621–640 (1997).
- Jenkins, J. T., and D. F. McTigue, "Transport process in concentrated suspensions: The role of particle fluctuations," Two Phase Flows and Waves, D. D. Joseph and D. G. Schaeffer, eds. (Springer, New York, 1990).
- Karnis, A., H. L. Goldsmith, and S. G. Mason, "The kinetics of flowing dispersions: I. Concentrated suspensions of rigid particles," J. Colloid Interface Sci. 22, 531–553 (1966).
- Koh, C. J., P. Hookman, and L. G. Leal, "An experimental investigation of concentrated suspension flows," J. Fluid Mech. 266, 1–32 (1994).
- Krieger, I. M., and T. J. Dougherty, "A mechanism for non Newtonian flow in suspensions of rigid spheres," Trans. Soc. Rheol. 3, 137–152 (1959).
- Krishnan, G. P., S. Beimfohr, and D. T. Leighton, "Shear-induced radial segregation in bidisperse suspensions," J. Fluid Mech. 321, 371–393 (1996).
- Leighton, D., and A. Acrivos, "The shear-induced migration of particles in concentrated suspensions," J. Fluid Mech. 181, 415–439 (1987).
- Leighton, D., and A. Acrivos, "Viscous resuspension," Chem. Eng. Sci. 41, 1377-1384 (1986).
- Lyon, M. K., and L. G. Leal, "An experimental study of the motion of concentrated suspensions in twodimensional channel flow: Part 1. Monodisperse systems," J. Fluid Mech. **363**, 25–56 (1998).
- Mills, P., and P. Snabre, "Rheology and structure of concentrated suspensions of hard spheres. Shear-induced particle migration," J. Phys. II 5, 1597–1608 (1995).
- Morris, J. F., and F. Boulay, "Curvilinear flows of non colloidal suspensions: The role of normal stresses," J. Rheol. **43**(5), 1213–1237 (1999).
- Morris, J. F., and J. F. Brady, "Pressure-driven flow of a suspension: Buoyancy effects," Int. J. Multiphase Flow **24**, 105–130 (1998).
- Nott, P. R., and J. F. Brady, "Pressure driven flow of suspensions: Simulation and theory," J. Fluid Mech. 275, 157–199 (1994).
- Patankar, S. V., Numerical Heat Transfer and Fluid Flow (Hemisphere, New York, 1980).
- Pesche, R., "Etude par simulation numérique de la ségrégation de particules dans une suspension bidisperse," PhD. thesis, Université de Nice Sophia-Antipolis (1998).
- Phillips, R. J., R. C. Armstrong, R. A. Brown, A. L. Graham, and J. R. Abbott, "A constitutive equation for concentrated suspensions that accounts for shear-induced particle migration," Phys. Fluids A 4, 30–40 (1992).
- Phung, T., "Behavior of concentrated colloidal suspensions by Stokesian dynamics simulation," Ph.D. thesis, Californian Institute of Technology (1993).
- Probstein, R. F., M. Z. Sengun, and T. C. Tseng, "Bimodal model of concentrated suspension viscosity for

distributed particle sizes," J. Rheol. 38, 811-829 (1994).

Sinton, S. W., and A. W. Chow, "NMR flow imaging of fluids and solid suspensions in Poiseuille flow," J. Rheol. 35, 735–772 (1991).

Tetlow, N., A. L. Graham, M. S. Ingber, S. R. Subia, L. A. Mondy, and S. A. Altobelli, "Particle migration in a Couette apparatus: Experiment and modeling," J. Rheol. **42**(2), 307–327 (1998).

Copyright of Journal of Rheology is the property of Society of Rheology and its content may not be copied or emailed to multiple sites or posted to a listsery without the copyright holder's express written permission. However, users may print, download, or email articles for individual use.